chemosensors

MDPI

Article

Rare Earth Element Detection and Quantification in Coal and Rock Mineral Matrices

Chet R. Bhatt [1,2,*], Daniel A. Hartzler [1] and Dustin L. McIntyre [1,*]

[1] National Energy Technology Laboratory, 3610 Collins Ferry Road, Morgantown, WV 26505, USA; daniel.hartzler@netl.doe.gov
[2] NETL Support Contractor, 3610 Collins Ferry Road, Morgantown, WV 26505, USA
* Correspondence: chet.bhatt@netl.doe.gov (C.R.B.); dustin.mcintyre@netl.doe.gov (D.L.M.)

Abstract

As global demand for rare earth elements (REEs) increases, maintaining the production and supply chain is critical. Technologies capable of being used in the field and in situ in the subsurface for rapid REE detection and quantification facilitates the efficient mining of known resources and exploration of new and unconventional resources. Laser-induced breakdown spectroscopy (LIBS) is a promising technique for rapid elemental analysis both in the laboratory and in the field. Multiple articles have been published evaluating LIBS for detection and quantification of REEs; however, REEs in their natural deposits have not been adequately studied. In this work, detection and quantification of two REEs, La and Nd, have been studied in both synthetic and natural mineral matrices at concentrations relevant to REE extraction. Measurements were performed on REE-containing rock and coal samples (natural and synthetic) utilizing different LIBS instruments and techniques, specifically a commercial benchtop instrument, a custom benchtop instrument (single- and double-pulse modes), and a custom LIBS probe currently being developed for in situ, subsurface, borehole wall detection and quantification of REEs. Plasma expansion, emission intensity, detection limits, and double-pulse signal enhancement were studied. The limits of detection (LOD) were found to be 10/14 ppm for La and 15/25 ppm for Nd in simulated coal/rock matrices in single-pulse mode. Signal enhancement of 3.5 to 6-fold was obtained with double-pulse mode as compared to single-pulse operation.

Keywords: laser-induced breakdown spectroscopy; REEs in coal; coal and rock minerals; La detection; Nd detection

check for updates

Received: 4 June 2025
Revised: 17 July 2025
Accepted: 18 July 2025
Published: 23 July 2025

Citation: Bhatt, C.R.; Hartzler, D.A.; McIntyre, D.L. Rare Earth Element Detection and Quantification in Coal and Rock Mineral Matrices. *Chemosensors* **2025**, *13*, 270. https://doi.org/10.3390/chemosensors13080270

Copyright: © 2025 by the authors. Licensee MDPI, Basel, Switzerland. This article is an open access article distributed under the terms and conditions of the Creative Commons Attribution (CC BY) license (https://creativecommons.org/licenses/by/4.0/).

1. Introduction

The United States Geological Survey (USGS) and U.S. Department of Energy (DOE) have declared rare earth elements (REEs) to be critically important materials. According to the Energy Act of 2020, any non-fuel materials that contribute to energy technology, economic and national security, and face a risk of supply chain disruption are considered critical materials and minerals [1]. In the periodic table, REEs are the 15 lanthanides (elements with atomic number ranging from 57 to 71) along with two transition elements scandium (21) and yttrium (39). Geologically, REEs are available in minerals mostly as trace constituents, though multiple REEs may occur in a single mineral. Major sources of minable REEs are carbonatites, alkaline igneous systems, ion-absorption clay deposits, and monazite-xenotime-bearing placer deposits, typically in low concentrations, with carbonatites (igneous rocks made of mostly carbonate) considered to be the largest sources

of REEs [2,3]. REEs are supremely important due to their diverse applications in modern technology. Critical optical and magnetic properties of REEs are useful for smart phones, televisions, petroleum refining, catalysts, power generation, military aircraft, computer memory drives, automotive systems, etc. [4–9]. Energy technologies such as electrical generators and motors use rare earth magnets as they are stronger than other types of magnets [10]. According to USGS Rare Earths Statistics and Information, mine production in the U.S. in 2024 was 45 thousand metric tons with an increase of 2000 metric tons compared to 2023 [11]. While the import decreased by 11% in its estimated value of rare earth compounds and metals in the year 2024 compared to the previous year, it still imported 8000 metric tons of these critical metal compounds. Global demand of rare earth oxides is approximately 118 thousand tons per year, which is estimated to reach 200 thousand tons per year by 2025 with a price estimated to be in the range of $110–150 thousand per ton [12–14]. Though a major share of rare earth deposits are located in China and other counties, the U.S. possesses significant reserves, estimated to be approximately 1.8 million metric tons [11]. With increasing demand and price, more REE resources are being explored and undiscovered resources are also possible due to advancements in engineering technologies for ore processing.

Sensing technologies enable exploration and evaluation of new or known REE resources, such as natural deposits or waste products. Major techniques currently used for REE measurement are inductively coupled plasma mass spectrometry (ICP-MS), inductively coupled plasma optical emission spectroscopy (ICP-OES), X-ray fluorescence (XRF), neutron activation analysis (NAA), etc. [15–19]. These are mostly laboratory-based techniques, requiring materials that need to be brought to the test centers for analysis. To evaluate REE content at the test sites, field-deployable, in situ techniques are more useful. Therefore, there is a critical need to develop sensors capable of rapid REE detection and quantification in non-laboratory environments. Recent studies have demonstrated LIBS as a good technique for field measurements [20–28]. Martin et al. have studied seven REEs (Eu, Gd, La, Nd, Pr, Sm, and Y) using their pure oxides [29]. While LIBS studies are mostly based on atomic and ionic emissions, application of laser-induced molecular emissions of the rare earth oxides is presented by Gaft et al. [30]. A review on REE determination by various spectroscopic techniques was published by Zawisza et al. [18]. Reported studies are mostly based on laboratory tests with standard samples; however, in real-world applications, REEs must be measured in natural ores which have complex matrices of multiple elemental species [8,31–34]. Therefore, it is valuable to study the behavior of laser-induced plasma emissions in various complex matrices. In our previous studies, multiple REEs, in both solids and aqueous solutions, have been studied using single- and double-pulse LIBS [35–38].

As our next aim is to develop a LIBS sensor for subsurface REE measurements by interrogating natural materials in situ within a borehole wall, in this study, selected REEs have been studied in both simulated and natural materials. The simulated samples were used to calibrate and optimize the LIBS system parameters, enabling the detection of La and Nd in test samples obtained from a natural REE deposit. Note that, in this study, the following definitions are used: “natural material” is material obtained from core samples of a coal seam and surrounding rock; “simulated material” is material produced in the lab to represent the approximate composition of the natural materials; “mineral phase” is all materials not lost on sample combustion (i.e., dry ash); “combustible” material is all materials lost on sample combustion; “coal-based” materials are materials that contain 0–10 wt.% dry ash; “rock-based” materials are 90–100% dry ash; “intermediate” or “mixed” materials are 10–90 wt.% dry ash (see Figure 1); “coal/rock mineral phase simulant” are the lab-produced materials approximating the corresponding natural mineral phases; and

"simulated coal/rock" or "coal/rock simulant" are lab-produced materials approximating the natural coal/rock-based materials.

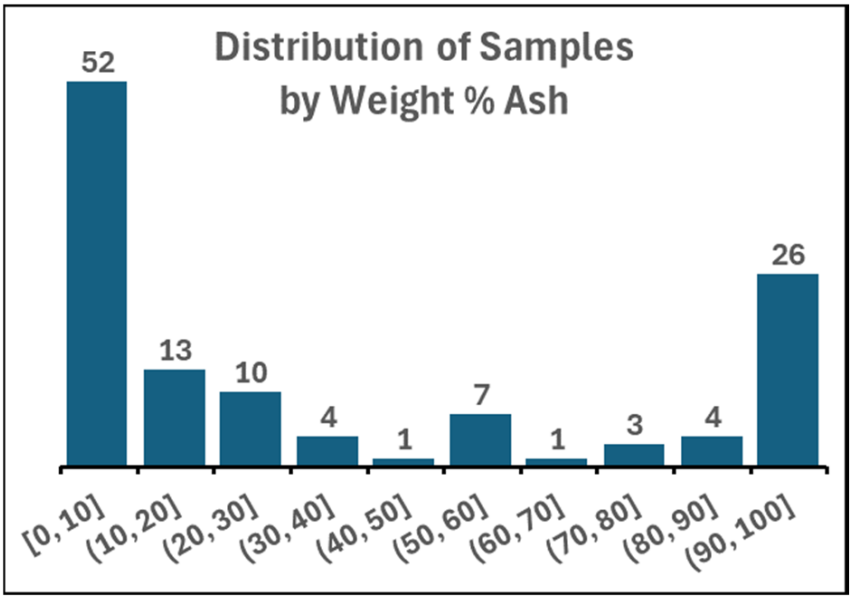


Figure 1. Distribution of ash (by wt.%) within the 121 natural samples. Based on this data, "coal-based" samples are defined as those with between 0–10 wt.% ash while "rock-based" samples are defined as having between 90–100 wt.% ash.

2. Materials and Methods

Natural coal and rock samples were obtained from a coal seam core known to contain REEs. The composition of these samples was determined through thermogravimetric analysis (TGA), ICP-MS, and ICP-OES (see the Supporting Information for the methods used). TGA was used to determine weight percentage (wt.%) moisture and dry ash, from which the wt.% of combustibles were calculated (wt.% combust = 100% − (% moisture) − (% dry ash)). For simplicity, it is assumed that all combustible material is 100% carbon. ICP-MS and ICP-OES were used to perform elemental analysis on the mineral phases contained within the samples, with aluminum (Al) determined via ICP-OES and the remainder determined via ICP-MS. The dry ash content of all 121 samples was between 3.1 and 95.2 wt.%, with 52 samples belonging to the "coal-based" category (defined earlier as materials containing 0–10 wt.% ash), 26 samples in the "rock-based" category (90–100 wt.% ash), and the remaining 43 samples belonging to the "intermediate" or "mixed" category. These categories were selected based on the distribution of ash within these samples (see Figure 1). Six samples named S-35, S-335, S-347, S-34, S-116, and S-154 were tested for the detection of selected REEs with four coal-based samples S-34 (5.54 wt.% ash), S-35 (6.72 wt.%), S-335 (6.46 wt.%), S-347 (5.44 wt.%); one rock-based sample S-116 (92.5 wt.% ash); and one mixed sample S-154 (37.28 wt.% ash). See Table 1 for their composition.

Simulated coal/rock-based samples resembling the natural test samples matrix were produced for calibration and system optimization. Based on the composition of all 121 natural samples, eight elements, all elements with an average concentration greater than 5000 ppm (Al, Na, Mg, Si, K, Ca, Fe) plus Ti (~4000 ppm), were selected to represent the mineral phases. Titanium was included because it is known to possess multiple emission lines throughout the spectral region of interest and, thus, has a high potential spectral interference. To produce the simulated coal and rock samples, mineral phase simulants were designed using the eight elements mentioned above to represent the approximate mineral phase composition of the natural-coal- and rock-based samples (Table 2). The

mineral phase simulants were then diluted with graphite (Table 3) to produce the final simulated coal and rock sample stock (Table 4). These two stock materials, "simulated coal" and "simulated rock," formed the basis of all simulant/calibration samples. Calibration samples for La and Nd were prepared by doping simulated coal/rock material with La_2O_3 and Nd_2O_3, with final dopant concentrations set to 125, 250, 500, and 1000 ppm (metal analyte concentration). One calibration set was produced for each analyte. Both calibration and natural samples were ground with a mortar and pestle to make a fine, homogeneous powder and pressed into pellets using 13 mm diameter die with a pellet press (Carver). While no binder was needed to press simulated coal samples, 20% starch was used as a binder for the simulated rock samples.

Table 1. Matrix composition and mineral phase REE composition of natural samples S-35, S-335, S-347, S-34, S-116, and S-154.

	Sample					
Name	**S-347**	**S-335**	**S-34**	**S-35**	**S-116**	**S-154**
Type	**Coal**	**Coal**	**Coal**	**Coal**	**Rock**	**Mixed**
Matrix Composition (ppm)						
Al †	54,840	43,690	107,100	125,900	101,100	148,500
Na	12,473	12,358	33,815	30,903	1081	4959
Mg	22,789	32,756	60,397	46,090	7951	13,064
Si	6972	44,595	90,935	129,393	326,740	274,680
K	1243	1709	3661	6332	20,344	15,203
Ca	206,800	263,307	146,943	101,674	3501	6669
Ti	1315	2472	2454	3458	5083	4939
Fe	69,950	63,177	29,709	25,058	32,341	36,275
TGA (wt.%)						
Moisture	32.88	17.35	16.19	19.78	1.90	13.79
Dry Ash	5.44	6.46	5.45	6.72	92.50	37.28
Combust. ‡	61.68	76.19	78.36	73.50	5.60	48.93
Mineral Phase REE Composition (ppm)						
Total Rare Earths						
REE + Sc + Y	1080	1980	1440	2500	310	950
Selected Rare Earths						
La	220	490	130	290	52	110
Nd	180	250	230	370	50	150

† Al determined through ICP-OES, remainder determined through ICP-MS. ‡ "Combust."/loss on combustion = 100% − Moisture wt.% − Dry Ash wt.%.

Table 2. Composition of coal and rock mineral phase and their simulants.

	Natural Mineral Phase		Mineral Phase Simulant	
	Coal	**Rock**	**Coal**	**Rock**
		Matrix Element (ppm)		
Al	75,270	111,593	74,300	100,000
Na	18,289	1600	29,600	2620
Mg	42,540	8569	38,900	8000
Si	74,367	344,342	81,400	320,000
K	2516	20,983	2480	20,000
Ca	186,483	5380	101,000	2870
Ti	2840	4969	3010	4600
Fe	50,195	23,832	49,500	22,000
		Dry Matter (wt.%)		
Ash †	7%	96%	--	--
Combust. ‡	93%	4%	--	--

†/‡ Weight % dry matter, where (†) Ash = (% Dry Ash)/(100% − % Moisture) and (‡) Combust. = 100% − % Dry Ash. Note that the average wt.% moisture of the coal-based samples was 17.5% and the rock-based samples was 3.3%.

Table 3. Recipe for simulated coal and rock matrices. Graphite is used to simulate the combustible component of the simulants.

	Coal Mineral Phase (wt.%)	Rock Mineral Phase (wt.%)
	Mineral Phase Simulant Component	
Al_2O_3	14.03	18.90
NaCl	5.58	0.49
$MgCO_3$	13.50	2.78
SiO_2	17.40	68.48
KCl	0.47	3.81
$CaCl_2 \cdot 2H_2O$	41.43	1.62
TiO_2	0.50	0.77
Fe_2O_3	7.08	3.15
	Dry Matter	
Mineral phase simulant	6	93
Graphite	94	7

Table 4. Simulated coal and rock matrix composition after dilution with graphite.

Matrix Element	Coal Simulant (ppm)	Rock Simulant (ppm)
Al	4460	93,000
Na	1780	2430
Mg	2330	7440
Si	4880	298,000
K	149	18,600
Ca	6090	2670
Ti	180	4280
Fe	2970	20,500
C	941,000 †	73,700 ‡

† 1200 ppm C and ‡ 3700 ppm C contributed by $MgCO_3$.

3. Principal Component Analysis of Test Samples

Broad spectrum data (185–900 nm) were acquired using a benchtop LIBS instrument (Applied Spectra J200, 266 nm laser, West Sacramento, CA, USA) from all samples; natural-coal- and rock-based samples and their simulants. Images of the sample pellets taken with the instrument's built-in microscope are shown in Figure 2. Note that coal-based samples were slightly darker than the rock-based samples. Principal Component Analysis (PCA) was performed using open-source software (Python 3.13.3) to evaluate if the samples can be distinguished using LIBS spectral data. Spectra for PCA were collected from 25 different spots on each pellet at 10 acquisitions per spot. Ten principal components were computed for PCA, the first two of which accounted for more than 90% of the total variance of the data. The clustering demonstrated by PCA clearly shows that the coal and rock simulants (Figure 3a) and the natural-coal- and rock-based samples (Figure 3b) cluster around similar values and, thus, can be categorized into their respective types. It must be noted that the mixed sample, S-154 (32.28 wt.% ash) was classified as "rock-based," which is likely due to the coal mineral phase being diluted within the carbon matrix; thus, the rock minerals provided a higher signal.

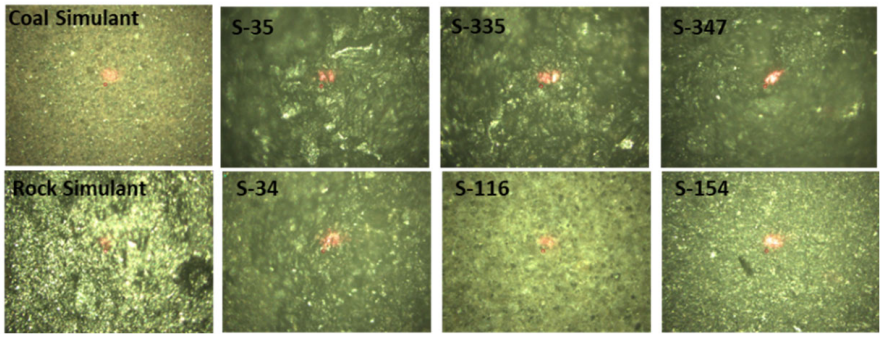


Figure 2. Images of the samples recorded using Applied Spectra's J200 in micro mode where S-34/35/335/347 are coal-based, S-116 is rock-based, and S-154 is intermediate/mixed. The coal and rock simulants pictured here are undoped materials.

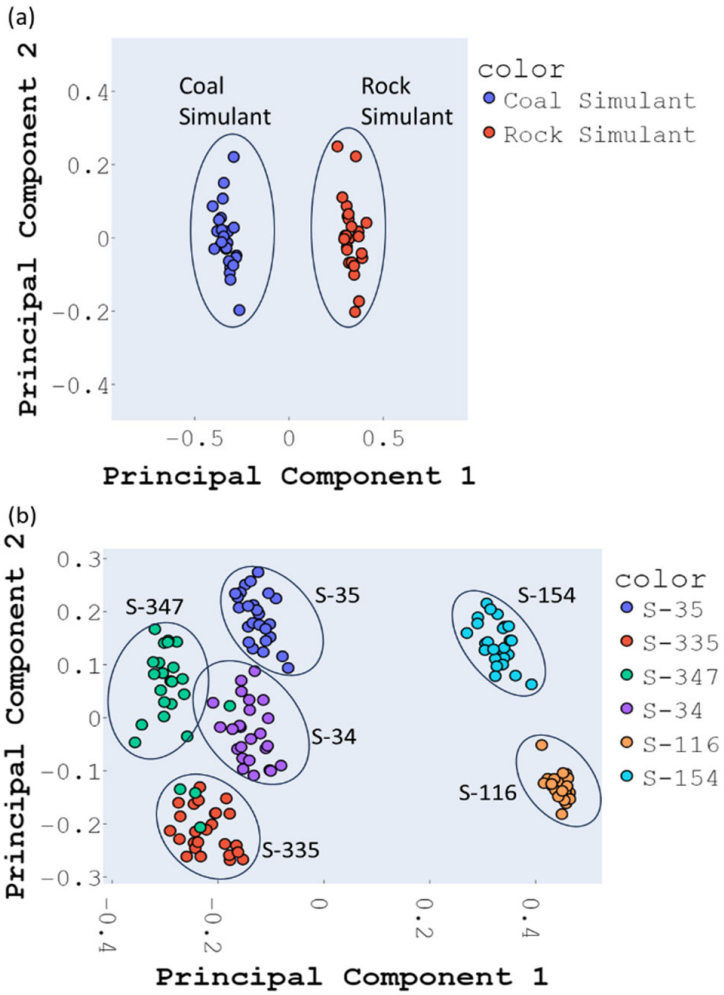


Figure 3. PCA showing the clustering of (**a**) coal and rock simulants, and (**b**) natural samples. Note that the analysis method identified the intermediate/"mixed" sample, S-154 (37.28 wt.% ash), as "rock-based" together with S-116 (92.50 wt.% ash) rather than "coal-based" like S-34/35/335/347 (5.44–6.72 wt.% ash).

4. LIBS Benchtop Experimental Setup

A custom benchtop LIBS setup was also used for the analysis (Figure 4). A 1064 nm Nd: YAG laser (New Wave Research, Fremont, CA, USA) producing pulses of 5 ns width was used as the excitation source and was focused with a 3.8 cm focal length lens on the surface of the sample pellets, which were placed on a rotating platform. A rotating platform was used so that each laser pulse would ablate fresh material from the sample pellet. The pulse energy delivered to the sample was adjusted using a half-wave plate and a polarizing beam splitter, and was kept fixed at 5 mJ per pulse. The plasma emission was collected in a confocal mode through the same focusing lens and directed using a dichroic mirror toward the collection lens (5 cm focal length) and fiber (Andor SR-OPT-8024, Thessaloniki, Greece). Plasma emissions were analyzed using a Czerny-Turner spectrograph (Andor Shamrock SR303i-A, Thessaloniki, Greece) with an intensified charge-coupled device (ICCD) camera (Andor iStar DH320T-25F-03, Thessaloniki, Greece).

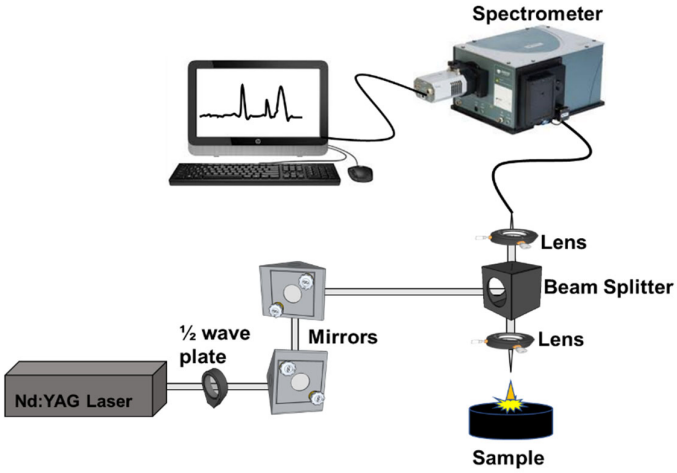


Figure 4. Experimental setup for benchtop LIBS measurements.

5. Detection and Selection of Characteristic Emission Lines

Selection of emission lines in LIBS spectra is critical to develop a sensing system for detection and measurement of REEs in natural sources. When LIBS spectra are obtained from materials with a complex composition, a number of emission lines of species present in the material may appear depending upon the matrix material and experimental parameters used. Ionic emission lines appear prominently with shorter gate time delays, while neutral emission lines are better detected at comparatively long gate time delays. Moreover, as different emission lines correspond to different excitation energies, the laser energy used for material ablation also plays an important role; however, higher laser energy carries a greater possibility of causing saturation in emission intensity. When a material has a complex composition (such as coal/rock), the emission lines of different elements might overlap with each other and cause spectral interference. As detection of elements of interest in the test materials primarily depend upon identification of the emission lines, interference-free emission lines are needed, particularly for trace elements which can be easily overwhelmed by matrix element emissions. This study aimed to analyze two trace REEs, specifically La and Nd. Based on the reported literature and the NIST database, the observed La and Nd emission lines in the 400–440 nm wavelength range are shown in Figure 5 [39–43]. After evaluating LIBS spectra recorded at various experimental, interference-free emission lines at 433.4 nm for La and 401.2 nm for Nd were chosen for the analysis of La and Nd in coal and rock matrices.

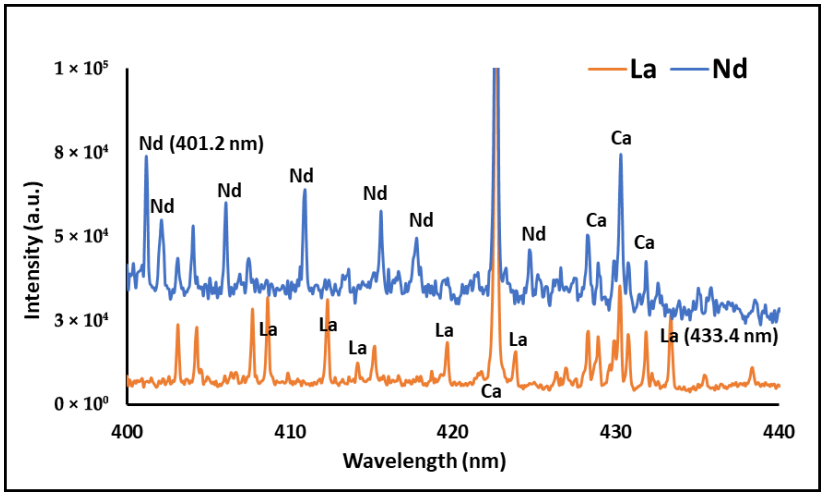


Figure 5. LIBS spectra showing La and Nd emission lines in the 400–440 nm wavelength range.

6. Temporal Evolution of Plasma Emission

When plasma is produced with laser-induced ablation, continuum emission is dominantly observed in the beginning due to bremsstrahlung and recombination processes in the plasma. As the plasma expands and cools, emission lines from ions, atoms, and then molecules appear subsequently. Therefore, to obtain ionic or atomic emission lines, a time delay after the plasma formation is needed to permit the plasma to cool sufficiently to obtain the desired lines and optimize signals. The temporal evolution of the plasma emissions in both coal and rock matrices for the selected La and Nd emission lines was studied. LIBS spectra were recorded at varying gate delay times at a fixed gate width/integration time (5 µs) and a fixed laser energy (5 mJ). Pulse energy was kept low to eliminate possible saturation and self-absorption seen at higher pulse energies. Gate delay was varied in the 0.1–10 µs range and emission signal peak intensity of both the La II 433.4 nm and Nd II 401.2 nm emission lines were monitored in simulated coal and rock matrices. Both the La and Nd signal peak intensity decreased almost exponentially with the increasing gate delay in both coal and rock matrices as shown in Figure 6a,c. When the signal peak intensity-to-background ratio (SBR) was plotted against the gate delay, it initially rapidly increased with increasing gate delay before slowly decreasing after reaching the maximum value as depicted in Figure 6b,d. While the absolute signal strength is high during the early stages of plasma emission, the background is also elevated due to the continuum emission, resulting in a low SBR. As time passes following plasma creation, the continuum emission decreases much more rapidly than the analyte emission intensity, causing the rise in, and eventual peak of, the SBR, as seen in Figure 6b,d. Interestingly, it was also noted that signal strength of both lines was found to be higher in the coal matrix compared to that in the rock matrix which might be attributed to the higher carbon content compared to other metals in the coal samples. For these samples, the peak SBR was found at a gate delay in the range of 0.5–3 µs for La II 433.4 nm and 0.5–4 µs for Nd II 401.2 nm lines. Therefore, this range of gate time delay was considered favorable to take LIBS spectra.

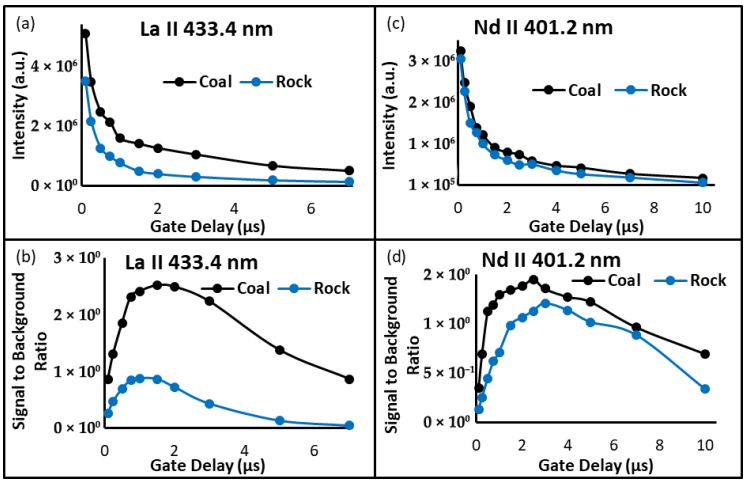


Figure 6. Variation of signal intensity and signal-to-background ratio (SBR) with increasing gate time delays. (**a**,**b**) for La II 433.4 nm and (**c**,**d**) for Nd II 401.2 nm emission lines.

7. Calibration Curves & Limits of Detection (LOD)

After finding the optimum experimental parameters (gate delay and analyte emission lines), univariate regression models were developed. These regression models were used to estimate limits of detection (LOD) of La and Nd in both coal and mineral simulants. As mentioned in Section 2, stock mixtures of the coal and rock simulants were doped with La and Nd oxides so that La and Nd concentrations were in the range of 125 ppm to 1000 ppm.

These powder samples were then pressed into pellets to perform measurements. Using the benchtop LIBS instrument (Figure 4), spectra were recorded from each of these sample pellets using a laser pulse of energy 5 mJ, a gate delay of 1 µs, and gate width of 5 µs. From each sample, 10 spectra were recorded with each spectrum consisting of 200 acquisitions. Background subtracted peak intensities of the emission lines, La II 433.4 nm and Nd II 401.2 nm, were plotted against the concentration to obtain linear regressions as shown in Figure 7. The coefficients of determination (R^2) values were found to be in the range 0.98–0.999 for all four calibration curves. *LOD* were estimated by using Equation (1):

$$LOD = 3\frac{\sigma}{S} \quad (1)$$

where σ is the standard deviation of the background—in this case it was taken from the blank sample—and S is the slope of the linear regression curve. The estimated LOD values (Table 5) were 10 ppm/14 ppm for La and 15 ppm/25 ppm for Nd in the simulated coal/rock materials, respectively. For both the analytes, La and Nd, estimated LOD values are lower in coal simulant compared to the rock simulant which can be attributed to the difference in their matrices. More precisely, physical properties like melting point, density, ionization energy, etc., of the species in the matrices with their different concentrations have a role in plasma formation, composition, and expansion which ultimately affects the plasma emission and hence detection limit. The possibility of a lower detection limit in the coal mineral simulant can also be expected by analyzing temporal evolution demonstrated in Figure 6 in the section "Temporal Evolution of Plasma Emission." For all the gate delays, the intensity of the analyte lines in the coal simulant is higher compared to the rock simulant.

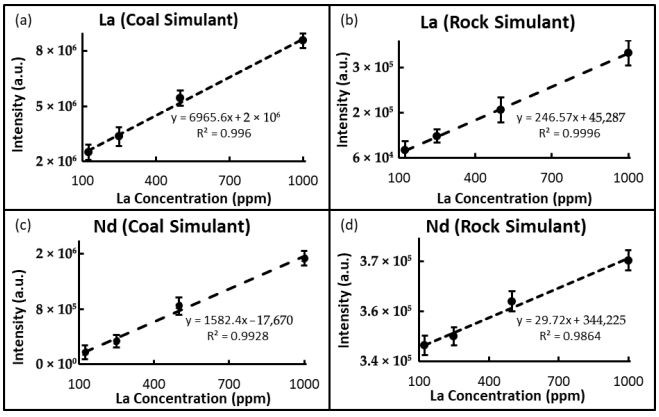


Figure 7. Calibration curves for La in (**a**) coal, (**b**) rock mineral simulants, and Nd in (**c**) coal, (**d**) rock mineral simulants.

Table 5. Detection limits (LODs) for La and Nd in simulated coal and rock materials.

Analyte	Matrix	
	Coal Simulant	**Rock Simulant**
La	10 ppm	14 ppm
Nd	15 ppm	25 ppm

8. REE Detection in Natural Samples

LIBS measurements were performed on six natural test samples to detect the presence of La and Nd. Four of these samples were coal-based (S-34/35/335/347), one was rock-based (S-116), and one was intermediate/mixed (S-154). See Table 1 for mineral phase REE concentrations. Samples consisted of finely powdered material which was subsequently

pressed into 13 mm pellets. It must be noted that, while the REE concentration was highest in the mineral phase of the coal-based samples, these samples only contained between 5.44–6.72 wt.% ash (Table 1). Therefore, one should expect the REE concentration in the as-extracted, natural material to be diluted by ~94 wt.% combustibles + moisture. LIBS spectra were recorded using a gate delay of 1 µs, a gate width of 5 µs, and a laser pulse energy of 5 mJ using the highest resolution setting (Grating 2400 l/mm) of the spectrometer. As mentioned before, samples were placed on a rotating platform and 10 spectra consisting of 200 acquisitions each were recorded. Spectral widths of 420–450 nm and 390–420 nm were used for La and Nd, respectively. La and Nd emission lines can be identified in the spectra of several samples (Figure 8). The La II 433.4 nm was detected in three coal-based samples, S-35/335/347, and the intermediate/mixed sample, S-154. Similarly, the Nd II 401.2 nm line was clearly identified in sample S-35 (coal-based), but only a very weak signal was detected (in the shoulder of a line from some other species) in the samples S-335/347 (coal-based) and the sample S-154 (mixed). Neither the La nor Nd emission lines were detected in the remaining two samples, S-37 (coal-based) and S-116 (rock-based).

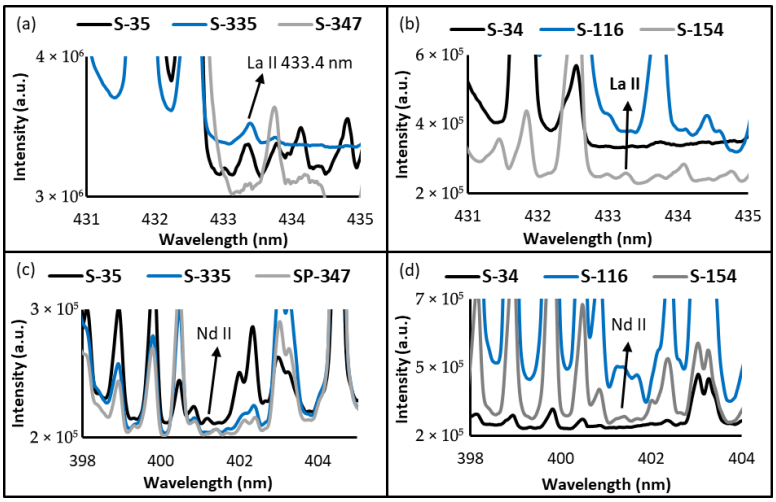


Figure 8. LIBS spectra showing La II 433.4 nm and Nd II 401.2 nm emission lines in the coal-based (S-34/35/335/347), rock-based (S-116), and intermediate (S-154) samples. (**a**,**c**) showing S-35/335/347 and (**b**,**d**) showing S-34/116/154.

9. Double Pulse LIBS for Signal Enhancement

For very low analyte concentrations, traditional single-pulse LIBS may not be adequate for analysis. In this situation, the double-pulse LIBS (DP-LIBS) signal enhancement technique might be useful, where two sequential laser pulses are used, increasing both the plasma volume and lifetime which attributes to stronger emission signals [44–49]. In this study, a collinear excitation mode DP-LIBS was applied to obtain stronger emission signals from the test samples. A second laser, identical to the one used in single-pulse benchtop setup (New Wave Research 1064 nm Nd: YAG laser, 5 ns width, Fremont, CA, USA), was used to reheat the plasma formed using the first laser after a short, inter-pulse delay. Both lasers were set to 5 mJ per pulse and the inter-pulse delay between the two lasers was controlled using a signal generator (Stanford Research System Inc DG535, Sunnyvale, CA, USA) with spectral acquisition being triggered together with the second laser. The inter-pulse delay was optimized to produce maximum signal-to-background ratio. For both La and Nd, an inter-pulse delay of 500 ns was found to contribute maximum signal enhancement compared to single-pulse LIBS and hence was chosen for all the measurements with the double-pulse setup. With respect to the second laser, gate delay was kept at 1 µs and gate width was kept at 5 µs. Using DP-LIBS, a significant enhancement of the analyte emission

lines was observed. With sample S-35 (Figure 9), the La and Nd emission lines were found to experience an intensity enhancement of 3.5 to 6-fold compared to the single-pulse LIBS technique. Additionally, the Nd emission signal in samples S-335/347/154 was also enhanced using the DP-LIBS technique; however, these lines are still partially obscured and appear as a shoulder on an emission line from some other species in the sample matrix as shown in Figure 10.

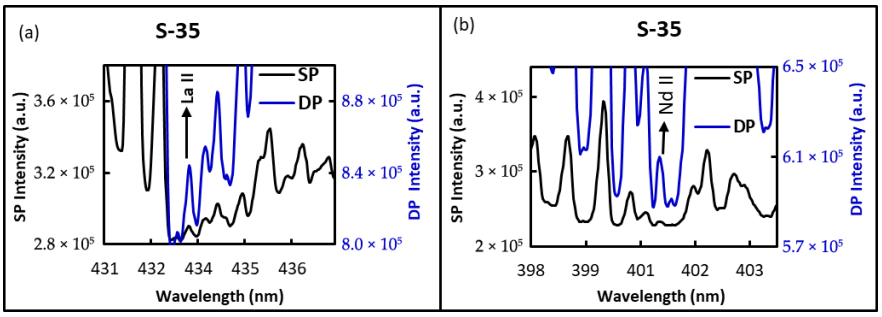


Figure 9. LIBS spectra showing signal enhancement with double-pulse LIBS. (**a**) La II emission line at 433.4 nm and (**b**) Nd II emission line at 401.2 nm.

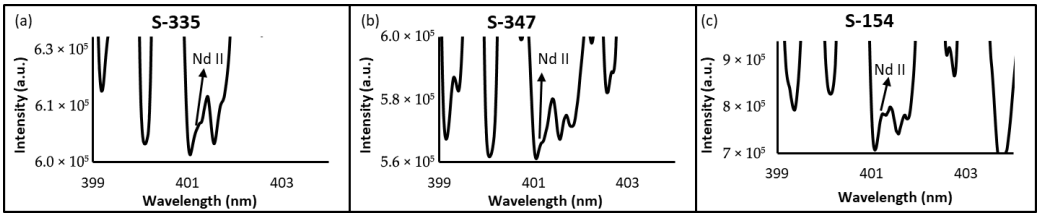


Figure 10. Nd II emission line at 401.2 nm detected with the double-pulse setup in samples (**a**) S-335, (**b**) S-347, and (**c**) S-154.

10. Measurements with LIBS-Prototype

A prototype of a LIBS-based sensor (see Hartzler et al. [36] for a description) under development for use in the subsurface was also evaluated for measurements of natural coal-based samples [50–52]. This sensor system splits the traditional benchtop LIBS system into two parts: (1) an all-optical sensor-head built around a passively Q-switched (PQSW) microchip (MC) laser (see Figure 11a,b)) which is connected via a fiber optic umbilical to (2) a control unit containing the spectrograph, pump-laser, etc. The sensor head's MC laser is pumped via fiber optic using a quasi-continuous wave (QCW) 808 nm diode laser (Lumibird Q1406-APF10, Lannion, France) and produces a 3 ns, 4 mJ laser pulse at 1064 nm. The MC laser output goes through beam expander, long-wave pass dichroic mirror (DCM), and then a focusing lens to interact with the test material to form a plasma. This laser-induced plasma emits light which is collected confocally and redirected using the DCM to a second optical fiber connected to the spectrograph. As with the benchtop setup, sample pellets were placed on a rotating platform for measurement. The laser pulse had 4 mJ energy, and gate time delay and integration time were set to be 1µs and 5µs, respectively. For each sample, 10 spectra consisting of 200 acquisitions each were recorded. Emission lines La II 433.4 nm and Nd II 401.2 nm were both detected in samples S-35 and S-335 but were not detected in S-347.

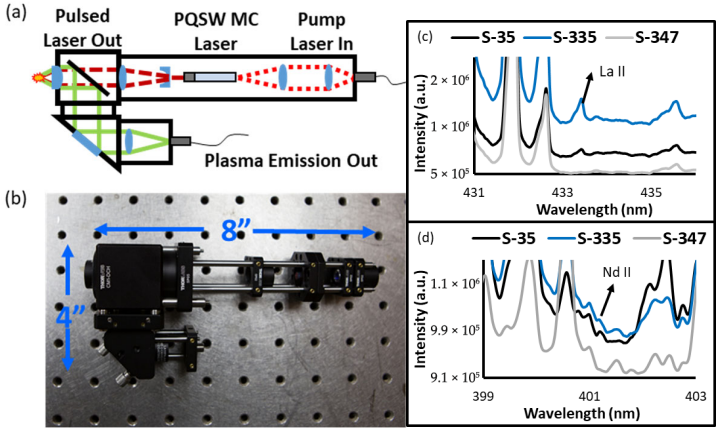


Figure 11. Schematic (**a**) and real (**b**) version of the prototype sensor head, LIBS spectra showing La (**c**) and Nd (**d**) emission signals.

This demonstrates the feasibility of using this type of instrument for REE detection, and potentially quantification, in natural materials. Given that the most recent iteration of the subsurface LIBS sensor head has an outer diameter (OD) of 2”/50.8 mm and is able to operate at well (and water) depths of up to 100 ft/30 m (having demonstrated operation at 30 ft/9 m well and 18 ft/5.5 m water depth, see reference [51]), it is feasible to develop a LIBS sensor capable of operating directly within a borehole to perform in situ measurements of the borehole wall. Work is underway to reduce the sensor head OD to permit operation in 2” boreholes.

11. Conclusions

LIBS was evaluated for the determination of REEs in their natural deposits, with La and Nd studied as a proof of concept. Two different sample matrices were tested, namely naturally occurring (and simulated) coal-based and rock-based material obtained from a natural REE deposit. Six natural samples and four sets of calibration samples (La/Nd doped simulated coal and La/Nd doped simulated rock) were tested to evaluate the performance of LIBS for detection of REEs in coal and rock matrices. Using the simulants, experimental parameters were evaluated to optimize La and Nd emission signals, and these signals were then detected in four of the six natural sample materials. PCA was performed, demonstrating the ability of LIBS + PCA to distinguish rock from coal-based materials and validating that the simulants replicated the natural materials. These experiments were performed with a variety of instrumentation, including a commercial benchtop LIBS system, a custom benchtop LIBS system capable of operating in single-pulse or double-pulse modes (SP/DP-LIBS), and a prototype LIBS sensor system under development for subsurface operation. The commercial instrument performed well for PCA classification due to its broad spectral acquisition window. The custom benchtop instrument (in single-pulse mode) demonstrated LODs of 10/14 ppm for La and 15/25 ppm for Nd in simulated coal/rock matrices, while double-pulse mode was used to demonstrate a 3.5 to 6-fold signal enhancement (in natural materials) as compared to single-pulse operation. Finally, the prototype subsurface LIBS sensor head demonstrated detection of La and Nd in natural coal-based material. Since versions of this prototype system have already been operated in the subsurface for over two weeks, this demonstrates the feasibility of using a LIBS-based sensor directly as a borehole for in situ detection and possibly for quantification of REEs.

Supplementary Materials: The following supporting information can be downloaded at: https://www.mdpi.com/article/10.3390/chemosensors13080270/s1, $LiBO_2$ Fusion Method; LECO 701

Thermogravimetric analysis (TGA) (Moisture& Ash); ICP-MS; and ICP-OES used by Pittsburgh analytical lab for the samples study.

Author Contributions: Conceptualization, C.R.B., D.A.H. and D.L.M.; methodology, validation, formal analysis, writing—original draft preparation, C.R.B. and D.A.H.; writing—review and editing, C.R.B., D.A.H. and D.L.M.; supervision, project administration, funding acquisition, D.L.M. All authors have read and agreed to the published version of the manuscript.

Funding: This project was funded by the United States Department of Energy, National Energy Technology Laboratory's Resource Sustainability Program.

Institutional Review Board Statement: Not applicable.

Informed Consent Statement: Not applicable.

Data Availability Statement: Data are contained within the article.

Acknowledgments: This work was performed in support of the U.S. Department of Energy's (DOE) Office of Fossil Energy and Carbon Management's Minerals Sustainability Program and executed through the National Energy Technology Laboratory (NETL) Research & Innovation Center's Critical Mineral Characterization Technologies Multi-Year Research Plan. Sample analysis by TGA, ICP-MS and ICP-OES were performed by NETL's Pittsburgh Analytical Laboratory (PAL).

Conflicts of Interest: The authors declare no conflicts of interest. This project was funded by the United States Department of Energy, National Energy Technology Laboratory, in part, through a site support contract. Neither the United States Government nor any agency thereof, nor any of their employees, nor the support contractor, nor any of their employees, makes any warranty, express or implied, or assumes any legal liability or responsibility for the accuracy, completeness, or usefulness of any information, apparatus, product, or process disclosed, or represents that its use would not infringe privately owned rights. Reference herein to any specific commercial product, process, or service by trade name, trademark, manufacturer, or otherwise does not necessarily constitute or imply its endorsement, recommendation, or favoring by the United States Government or any agency thereof. The views and opinions of authors expressed herein do not necessarily state or reflect those of the United States Government or any agency thereof.

References

1. What Are Critical Materials and Critical Minerals? Available online: https://www.energy.gov/cmm/what-are-critical-materials-and-critical-minerals (accessed on 2 August 2024).
2. Schulz, K.J.; DeYoung, J.H., Jr.; Seal, R.R., II; Bradley, D. Critical Mineral Resources of the United States—An Introduction. US Geological Survey: Reston, VA, USA, 2017.
3. Schulz, K.J.; DeYoung, J.H., Jr.; Seal, R.R., II; Bradley, D. Critical Mineral Resources of the United States: Economic and Environmental Geology and Prospects for Future Supply. US Geological Survey: Reston, VA, USA, 2017.
4. Suli, L.M.; Ibrahim, W.H.W.; Aziz, B.A.; Deraman, M.R.; Ismail, N.A. A review of rare earth mineral processing technology. *Chem. Eng. Res. Bull.* **2017**, *19*, 20–35. [CrossRef]
5. Lucas, J.; Lucas, P.; Le Mercier, T.; Rollat, A.; Davenport, W.G. *Rare Earths: Science, Technology, Production and Use*; Elsevier: Amsterdam, The Netherlands, 2014.
6. Omodara, L.; Pitkäaho, S.; Turpeinen, E.M.; Saavalainen, P.; Oravisjärvi, K.; Keiski, R.L. Recycling and substitution of light rare earth elements, cerium, lanthanum, neodymium, and praseodymium from end-of-life applications—A review. *J. Clean. Prod.* **2019**, *236*, 117573. [CrossRef]
7. Reddy, R.R. Prospective Potential Applications and Emerging Tendencies in Rare Earth Materials. In *Rare Earth: A Tribute to the Late Mr. Rare Earth, Professor Karl Gschneidner*; Materials. In *Rare Earth: A Tribute to the Late Mr. Rare Earth, Professor Karl Gschneidner*; Materials Research Forum: Millersville, PA, USA, 2024.
8. Balaram, V. Sources and Applications of Rare Earth Elements. In *Environmental Technologies to Treat Rare Earth Elements Pollution: Principles and Engineering*; IWA Publishing: London, UK, 2022.
9. Bhatt, C.R.; Jain, J.C.; Goueguel, C.L.; Mclntyre, D.L. Determination of rare earth elements in geological samples using laser-induced breakdown spectroscopy (LIBS). *Appl. Spectrosc.* **2018**, *72*, 114–121. [CrossRef]
10. Van Gosen, B.S.; Verplanck, P.L.; Long, K.R.; Gambogo, J.; Seal, R.R., II. The Rare-Earth Elements: Vital to Modern Technologies and Lifestyles. In *Fact Sheet*; USGS Mineral Resources Program: Reston, VA, USA, 2014; p. 4.

11. USGS. Rare Earths Statistics and Information. Available online: https://www.usgs.gov/centers/national-minerals-information-center/rare-earths-statistics-and-information (accessed on 15 May 2025).
12. Alonso, E.; Sherman, A.M.; Wallington, T.J.; Everson, M.P.; Field, F.R.; Roth, R.; Kirchain, R.E. Evaluating rare earth element availability: A case with revolutionary demand from clean technologies. *Environ. Sci. Technol.* **2012**, *46*, 3406–3414. [CrossRef]
13. Dutta, T.; Kim, K.H.; Uchimiya, M.; Kwon, E.E.; Jeon, B.H.; Deep, A.; Yun, S.T. Global demand for rare earth resources and strategies for green mining. *Environ. Res.* **2016**, *150*, 182–190. [CrossRef]
14. Yadav, J.; Sarker, S.K.; Bruckard, W.; Jegatheesan, V.; Haque, N.; Singh, N.; Pramanik, B.K. Greening the Supply Chain: Sustainable Approaches for Rare Earth Element Recovery from Neodymium Iron Boron Magnet Waste. *J. Environ. Chem. Eng.* **2024**, *12*, 113169. [CrossRef]
15. Verma, S.P.; Santoyo, E.; Velasco-Tapia, F. Statistical evaluation of analytical methods for the determination of rare-earth elements in geological materials and implications for detection limits. *Int. Geol. Rev.* **2002**, *44*, 287–335. [CrossRef]
16. Hall, G.E.; Vaive, J.E.; McConnell, J.W. Development and application of a sensitive and rapid analytical method to determine the rare-earth elements in surface waters. *Chem. Geol.* **1995**, *120*, 91–109. [CrossRef]
17. Golloch, A. *Handbook of Rare Earth Elements: Analytics*; Walter de Gruyter GmbH & Co KG: Berlin, Germany, 2022.
18. Zawisza, B.; Pytlakowska, K.; Feist, B.; Polowniak, M.; Kita, A.; Sitko, R. Determination of rare earth elements by spectroscopic techniques: A review. *J. Anal. At. Spectrom.* **2011**, *26*, 2373–2390. [CrossRef]
19. Whitty-Léveillé, L.; Turgeon, K.; Bazin, C.; Larivière, D. A comparative study of sample dissolution techniques and plasma-based instruments for the precise and accurate quantification of REEs in mineral matrices. *Anal. Chim. Acta* **2017**, *961*, 33–41. [CrossRef]
20. Zhiwei, D.E.N.G.; Sutong, G.U.O.; Zhishuai, X.U.; Ziyi, Z.H.A.O.; Ying, L.U.; Li, L.I.U.; Zhongqi, H.A.O. Quantitative Analysis of Rare Earth Elements Based on Double-pulse LIBS Combined with Partial Least Squares Regression. *Chin. J. Inorg. Anal. Chem./Zhongguo Wuji Fenxi Huaxue* **2024**, *14*, 183.
21. Zhou, J.; Hu, S.; Ren, X.; Li, M.; Xu, Y.; Zhang, T.; Tang, H.; Li, H. Rapid quantitative analysis of multiple rare earth elements in NdFeB alloys based on laser-induced breakdown spectroscopy (LIBS) and random forest (RF). *Spectrochim. Acta Part B At. Spectrosc.* **2024**, *217*, 106957. [CrossRef]
22. Fayyaz, A.; Asghar, H.; Alshehri, A.M.; Alrebdi, T.A. LIBS assisted PCA analysis of multiple rare-earth elements (La, Ce, Nd, Sm, and Yb) in phosphorite deposits. *Heliyon* **2023**, *9*, e13957. [CrossRef] [PubMed]
23. Rethfeldt, N.; Brinkmann, P.; Riebe, D.; Beitz, T.; Köllner, N.; Altenberger, U.; Löhmannsröben, H.G. Detection of rare earth elements in minerals and soils by laser-induced breakdown spectroscopy (LIBS) using interval PLS. *Minerals* **2021**, *11*, 1379. [CrossRef]
24. Harmon, R.S.; De Lucia, F.C.; Miziolek, A.W.; McNesby, K.L.; Walters, R.A.; French, P.D. Laser-induced breakdown spectroscopy (LIBS)–an emerging field-portable sensor technology for real-time, in-situ geochemical and environmental analysis. *Geochem. Explor. Environ. Anal.* **2005**, *5*, 21–28. [CrossRef]
25. Yamazaki, A.; Orikasa, Y.; Chen, K.; Uchimoto, Y.; Kamiya, T.; Koka, M.; Satoh, T.; Mima, K.; Kato, Y.; Fujita, K. In-Situ measurement of the Lithium Distribution in Li-Ion Batteries Using Micro-IBA Techniques. In *Nuclear Instruments and Methods in Physics Research Section B: Beam Interactions with Materials and Atoms*; Elsevier: Amsterdam, The Netherlands, 2016.
26. Samek, O.; Beddows, D.C.; Kaiser, J.; Kukhlevsky, S.V.; Liska, M.; Telle, H.H.; Whitehouse, A.J. Application of laser-induced breakdown spectroscopy to in situ analysis of liquid samples. *Opt. Eng.* **2000**, *39*, 2248–2262. [CrossRef]
27. Theriault, G.A.; Bodensteiner, S.; Lieberman, S.H. A real-time fiber-optic LIBS probe for the in situ delineation of metals in soils. *Field Anal. Chem. Technol.* **1998**, *2*, 117–125. [CrossRef]
28. Fabre, C.; Ourti, N.E.; Ballouard, C.; Mercadier, J.; Cauzid, J. Handheld LIBS analysis for in situ quantification of Li and detection of the trace elements (Be, Rb and Cs). *J. Geochem. Explor.* **2022**, *236*, 106979. [CrossRef]
29. Martin, M.Z.; Labbé, N.; André, N.; Harris, R.; Ebinger, M.; Wullschleger, S.D.; Vass, A.A. High resolution applications of laser-induced breakdown spectroscopy for environmental and forensic applications. *Spectrochim. Acta Part B At. Spectrosc.* **2007**, *62*, 1426–1432. [CrossRef]
30. Gaft, M.; Nagli, L.; Gorychev, A.; Raichlin, Y. Rare-earth elements detection using diatomic molecular laser-induced plasma spectroscopy. *Spectrochim. Acta Part B At. Spectrosc.* **2022**, *192*, 106426. [CrossRef]
31. Gaustad, G.; Williams, E.; Leader, A. Rare earth metals from secondary sources: Review of potential supply from waste and byproducts. *Resour. Conserv. Recycl.* **2021**, *167*, 105213. [CrossRef]
32. Van Gosen, B.S.; Verplanck, P.L.; Seal, R.R., II; Long, K.R.; Gambogi, J. *Rare-Earth Elements*; US Geological Survey: Reston, VA, USA, 2017.
33. Liu, S.L.; Fan, H.R.; Liu, X.; Meng, J.; Butcher, A.R.; Yann, L.; Yang, K.F.; Li, X.C. Global rare earth elements projects: New developments and supply chains. *Ore Geol. Rev.* **2023**, *157*, 105428. [CrossRef]
34. Goodenough, K.M.; Wall, F.; Merriman, D. The rare earth elements: Demand, global resources, and challenges for resourcing future generations. *Nat. Resour. Res.* **2018**, *27*, 201–216. [CrossRef]

35. Bhatt, C.R.; Yueh, F.Y.; Singh, J.P. Univariate and multivariate analyses of rare earth elements by laser-induced breakdown spectroscopy. *Appl. Opt.* **2017**, *56*, 2280–2287. [CrossRef]
36. Hartzler, D.A.; Bhatt, C.R.; Jain, J.C.; McIntyre, D.L. Evaluating laser-induced breakdown spectroscopy sensor technology for rapid source characterization of rare earth elements. *J. Energy Resour. Technol.* **2019**, *141*, 070704. [CrossRef]
37. Bhatt, C.R.; Jain, J.C.; Goueguel, C.L.; McIntyre, D.L.; Singh, J.P. Measurement of Eu and Yb in aqueous solutions by underwater laser induced breakdown spectroscopy. *Spectrochim. Acta Part B At. Spectrosc.* **2017**, *137*, 8–12. [CrossRef]
38. Bhatt, C.R.; Jain, J.C.; Bol'shakov, A.A.; McIntyre, D.L. Chemistry imaging and distribution analysis of rare earth elements in coal using LIBS and LA-ICP-MS instruments. *Int. J. Coal Geol.* **2025**, *301*, 104710. [CrossRef]
39. Martin, M.; Martin, R.C.; Allman, S.; Brice, D.; Wymore, A.; Andre, N. Quantification of rare earth elements using laser-induced breakdown spectroscopy. *Spectrochim. Acta Part B At. Spectrosc.* **2015**, *114*, 65–73. [CrossRef]
40. Edahbi, M.; Plante, B.; Benzaazoua, M.; Kormos, L.; Pelletier, M. Rare earth elements (La, Ce, Pr, Nd, and Sm) from a carbonatite deposit: Mineralogical characterization and geochemical behavior. *Minerals* **2018**, *8*, 55. [CrossRef]
41. NIST Atomic Spectra Database. Available online: https://www.nist.gov/pml/atomic-spectra-database (accessed on 15 May 2025).
42. Unnikrishnan, V.K.; Nayak, R.; Devangad, P.; Tamboli, M.M.; Santhosh, C.; Kumar, G.A.; Sardar, D.K. Calibration based laser-induced breakdown spectroscopy (LIBS) for quantitative analysis of doped rare earth elements in phosphors. *Mater. Lett.* **2013**, *107*, 322–324. [CrossRef]
43. Wang, D.; Zhang, A.; Zeng, J.; Wang, X. Quantitative analysis of rare earth elements in lanthanum and cerium carbonate by LIBS metho. *EMU* **2024**, *120*, 65.
44. Ahmed, R.; Baig, M.A. A comparative study of single and double pulse laser induced breakdown spectroscopy. *J. Appl. Phys.* **2009**, *106*, 033307. [CrossRef]
45. Bhatt, C.R.; Hartzler, D.; Jain, J.C.; McIntyre, D.L. Evaluation of analytical performance of double pulse laser-induced breakdown spectroscopy for the detection of rare earth elements. *Opt. Laser Technol.* **2020**, *126*, 106110. [CrossRef]
46. Stratis, D.N.; Eland, K.L.; Angel, S.M. Dual-pulse LIBS using a pre-ablation spark for enhanced ablation and emission. *Appl. Spectrosc.* **2000**, *54*, 1270–1274. [CrossRef]
47. Babushok, V.I.; DeLucia, F.C., Jr.; Gottfried, J.L.; Munson, C.A.; Miziolek, A.W. Double pulse laser ablation and plasma: Laser induced breakdown spectroscopy signal enhancement. *Spectrochim. Acta Part B At. Spectrosc.* **2006**, *61*, 999–1014. [CrossRef]
48. Scaffidi, J.; Angel, S.M.; Cremers, D.A. Emission Enhancement Mechanisms in Dual-Pulse LIBS. ACS Publications: Washington, DC, USA, 2006.
49. Nicolodelli, G.; Senesi, G.S.; Romano, R.A.; de Oliveira Perazzoli, I.L.; Milori, D.M.B.P. Signal enhancement in collinear double-pulse laser-induced breakdown spectroscopy applied to different soils. *Spectrochim. Acta Part B At. Spectrosc.* **2015**, *111*, 23–29. [CrossRef]
50. Hartzler, D.A.; Jain, J.C.; McIntyre, D.L. Development of a subsurface LIBS sensor for in situ groundwater quality monitoring with applications in CO_2 leak sensing in carbon sequestration. *Sci. Rep.* **2019**, *9*, 4430. [CrossRef]
51. Hartzler, D.A.; Bhatt, C.R.; McIntyre, D.L. Design, construction, and validation of an in-situ groundwater trace element analyzer with applications in carbon storage. *Sci. Rep.* **2023**, *13*, 7516. [CrossRef]
52. Hartzler, D.A.; Bhatt, C.R.; McIntyre, D. *All Optical Subsurface Elemental Analysis Probe*; National Energy Technology Laboratory (NETL): Pittsburgh, PA, USA; Morgantown, WV, USA; Albany, OR, USA, 2022.

Disclaimer/Publisher's Note: The statements, opinions and data contained in all publications are solely those of the individual author(s) and contributor(s) and not of MDPI and/or the editor(s). MDPI and/or the editor(s) disclaim responsibility for any injury to people or property resulting from any ideas, methods, instructions or products referred to in the content.